Geochemical Perspectives Letters

Onset of new, progressive crustal growth in the central Slave craton at 3.55 Ga

J.R. Reimink, D.G. Pearson, S.B. Shirey, R.W. Carlson, J.W.F. Ketchum

Supplementary Information

The Supplementary Information includes:

- Elemental Compositions
- Ages and Zircon Characteristics
- Comparison and Reinterpretation of Previous Detrital Zircon Data
- Hafnium-isotope Data from the AGC
- Sample Descriptions and Methods
- Sample Descriptions
- Sample Preparation
- LA-ICPMS Methods
- Data Reduction Notes
- U-Pb-Hf Isotope Summary for Each Sample
- Supplemental Methods Regarding U-Pb-Hf Isotope Data Treatment
- Tables S-1 and S-2
- Figures S-1 to S-4
- Supplementary Information References

Elemental Compositions

These samples span a wide range of major element compositions, with SiO_2 ranging from 58–77 wt. %. The majority have high Na_2O/K_2O, from 0.9–4.5. In general, the CSBC granitoids analysed here are mostly trondhjemites (Fig. 1), though some samples have higher CaO or K_2O contents than typical Archean TTGs (tonalite-trondhjemite-granodiorite). The three samples analysed in this study from Acasta (JR16-101;102;103) are all similar to previously documented <3.6 Ga granitoids in the AGC (Reimink *et al.*, 2016a), and nearly identical to a ~3.4 Ga sample documented in that work (JR13-802).

The CSBC rocks have trace-element patterns typical of Archean TTGs with enrichments in the large-ion-lithophile elements (Rb, U, Th), depletions in Nb and Ta, as well as Pb enrichments. There are highly variable REE contents among samples in this suite, with La/Yb ranging from 12–152. Both positive and negative Eu-anomalies are present, although several have no Eu anomaly.

Ages and Zircon Characteristics

Both CSBC and AGC samples analysed here have ages that correspond to the major magmatic pulses discussed in the main text, including the 3.4–3.3 Ga, and 2.95 Ga events. Several CSBC samples contain xenocrystic zircon cores representing crustal recycling in some form, either by inheritance from their sources during partial melting, or by assimilation of country rock into the magma upon emplacement. No xenocrystic cores were found to be older than 3.4 Ga. Several magmatic events within the CSBC and AGC have nearly identical ages which argues for the proximity of these crustal blocks to each other. These events are ~3.3–3.4 Ga (Acasta samples JR16-102, 103, JR13-802 as well as samples documented by Bauer *et al.*, 2017; CSBC samples JR16-329, 333), and ~2.95 Ga (AGC samples JR13-304 and samples from Bauer *et al.*, 2017; CSBC samples JR16-512, 517, 519, 406). Zircon Hf-isotope compositions from CSBC granitoids are complex due to the polymetamorphic nature of these rocks and several samples contain multiple generations of magmatic zircon. For these samples we assigned ages and ε_{Hf} values to multiple populations after checking for Pb-loss using combined U-Pb-Hf systematics. No systematic geographical variations in ε_{Hf} are apparent within the CSBC dataset, though differences are seen between these rocks and those of the AGC.

Comparison and Reinterpretation of Previous Detrital Zircon Data

Pietranik *et al.* (2008) analysed 137 detrital zircons extracted from the sedimentary cover group that directly overlies the Central Slave Basement Complex samples (Sircombe *et al.*, 2001) for their Hf-isotope compositions. Using a combination of Hf- and O-isotope analyses, these authors concluded that the Slave craton basement gneiss complex was formed by episodic mafic crust extraction from the mantle, followed by extended reworking of this mafic crust. They suggested that zircons extracted from the Slave craton with $\delta^{18}O$ values indistinguishable from the mantle field had clear peaks in depleted-mantle Hf-extraction ages. Their conclusions are very different from our inference, based on igneous-sample derived zircon Hf-isotope data, that the bulk of the Slave craton basement gneisses were formed by progressive extraction from 3.55–2.9 Ga. In an attempt to rectify these two interpretations, we plot the detrital zircon Hf-isotope data by location, and compare to our inferences that the AGC and CSBC have distinctly different Hf-isotope signatures.

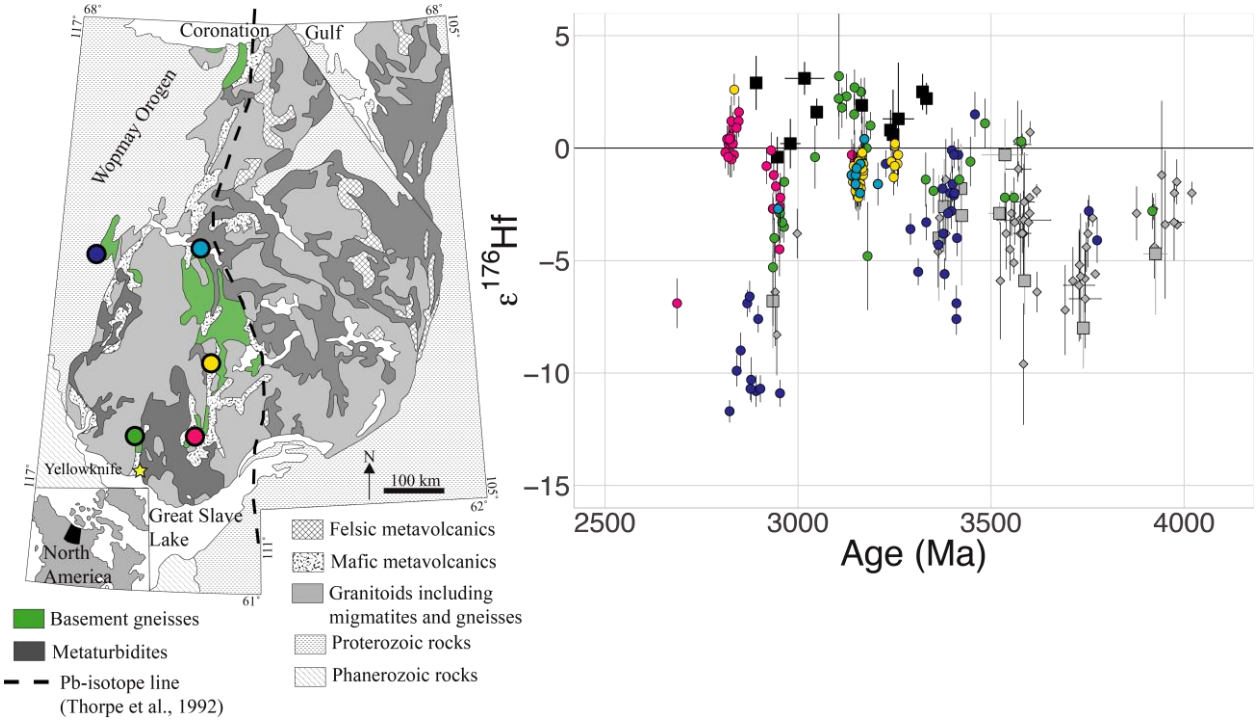

Figure S-1 Detrital zircon U-Pb-Hf isotope data from Pietranik *et al.* (2008) compared to our data from magmatic rocks. Grey symbols are from Acasta (diamonds from the compilation described in the main text, squares from the new data presented here). Black squares are the CSBC data presented in this work. Circles are detrital zircon data coloured by location, as on the map on the left. The green and purple locations (Exmouth Lake and Dwyer Lake, respectively) are grouped as "Western Slave detrital" in Figure 3 of the main text, while the pink, yellow, and light blue locations (Patterson, Loop, and Point Lakes, respectively) are grouped as "Eastern Slave detrital".

Here, as in Figure 3, colours correspond to detrital zircon sample location, except we have broken up the five sample locations into five groups. The grey symbols correspond to the same Acasta samples as in Figure 3, while the black squares are the CSBC data. Coloured circles are the detrital zircon data from Petranik *et al.* (2008), coloured by sample locations identified on the map. As in Figure 3, it is clear that all the >3.4 Ga grains, and nearly all grains with εHf values <-5 are restricted to the westernmost sample locations. One sample, Exmouth Lake (dark blue), sits directly on the AGC, and another, Dwyer Lake (green symbol) is from an area that is known to contain isotopic signatures indicative of the presence of AGC-aged crust (*e.g.*, Thorpe, 1992; Yamashita *et al.*, 1999). As the sediments deposited on the basement gneisses are interpreted to be rift-related sediments, they likely include detrital zircons from local sources (*e.g.*, Bleeker *et al.*, 1999; Sircombe *et al.*, 2001), and therefore are not representative of the broader Slave craton evolution. Our new basement gneiss data, when combined with a sample-by-sample analyses of the age-εHf relationships in the detrital zircon dataset, seems to validate this interpretation.

Our basement gneiss data suggests progressive tapping of a depleted mantle source (or close to the depeleted mantle composition) from 3.55 Ga onwards (Fig. 3) and our interpretation for the low εHf values in AGC rocks that are 3.4 and 2.95 Ga (-3 and -7, respectively) posits that juvenile depleted mantle material was simply mixing (via assimilation) with ancient, evolved, felsic crust. Older xenocrystic zircons in 3.4 Ga AGC rocks is further evidence for this process occurring. When the detrital zircon data is broken up by sediment location (Figs. 3 and S-1), the geographical similarities between CSBC and CSBC-derived sediments in age-εHf space, and similarities between AGC and AGC-derived sediments in the same space, imply that the regional differences seen in our igneous-sample based Hf data are robust.

Hafnium-isotope Data from the AGC

A substantial amount of Hf-isotope data has been collected from the AGC so far, summarised in some detail by Bauer *et al.* (2017), we provide the full list of references here: Amelin *et al.*, 1999; Amelin *et al.*, 2000; Bauer *et al.*, 2017; Guitreau *et al.*, 2012; Guitreau *et al.*, 2014; Iizuka and Hirata, 2005; Iizuka *et al.*, 2009; Reimink *et al.*, 2016b.

Sample Descriptions and Methods

During the summer of 2016 we collected several dozen samples of orthogneiss from the AGC and CSBC, in areas highlighted in Figure 1. Samples were selected for further analysis based on relative lithological homogeneity, lack of clear alteration products such as epidote veining and seriticisation, and preservation of igneous zircon. A subset of samples was processed for bulk geochemistry and zircon separation. Zircon from these samples were analysed by split-stream LA-ICPMS (LASS) methods at the University of Alberta in January of 2018 following the methods described in Reimink *et al.* (2016b). Zircons from seven samples described by Reimink *et al.* (2016a) were analysed in June of 2015 using identical LASS methods.

Sample Preparation

Samples were initially processed by slabbing 0.5–1.5 kg of hand sample, removing areas with obvious weathering or alteration, breaking slabs with a hammer, and crushing in an alumina jaw crusher. An aliquot of sample chips was sent to Washington State University's Geoanalytical Laboratory and crushed for elemental analysis using XRF and ICPMS.

Sample Descriptions

For descriptions of most of the Acasta samples analysed here, see Reimink *et al.* (2016a).

Samples from Acasta, ~10km SW of the discovery area

JR16-101

This sample comes from a large body of homogeneous, pink-coloured, foliated granodiorite containing mainly quartz, feldspar, and biotite. Veins of potassium feldspar and quartz cross-cut the outcrops, but within each outcrop the rock is a homogenous granodiorite, on the scale of tens of metres.

JR16-102

This sample is from a large body of homogeneous, pink-white, foliated granodiorite that has slightly more biotite than the previous sample. Outcrops have some epidote veining, though it is not pervasive. Rock contains mainly quartz, feldspar, and biotite.

JR16-103

This sample comes from a smaller body (~10 metres) of white granite that is near the sample locations described above (see GPS coordinates). This granite contains abundant quartz, feldspar, and biotite.

Samples from the Point Lake area in the CSBC

JR16-213

This sample is from a small, ~10 cm-wide, layer of banded gneiss that had been previously sampled by John Ketchum. This particular sample is a layer of darker tonalite, containing quartz, plagioclase, and a high proportion of biotite and amphibole. The gneissic fabric in this rock is defined by quartz-rich layers alternating with more leucocratic layers at the cm-scale.

JR16-215

Sample of a homogenous, foliated, quartz-diorite. This unit is cross-cut by coarse quartz-feldspar pegmatites across much of the outcrop. The sample of the quartz diorite contains a high proportion of amphibole and biotite, as well as plagioclase and quartz.

JR16-217

Sample of a fine-grained, light grey tonalite containing amphibole, plagioclase, biotite, and quartz and is associated with the quartz diorite sampled in JR16-215. Both of these samples are foliated and cross-cut by pegmatites.

JR16-236

This is a sample of the more evolved phase in the Augustus Granitoid complex. As such, it is coarse grained and heavily altered, containing abundant calcite, chlorite, and epidote-group minerals. The main portion of the rock is made up of quartz and plagioclase, with amphibole and biotite that have been altered to biotite and chlorite. The calcite and epidote occurs within veins and the plagioclase has been heavily sericitised.

JR16-254

This sample is a fine-grained granodiorite containing a small proportion of biotite and amphibole, with abundant plagioclase and quartz. Titanite is a common accessory mineral. Grain boundaries are mostly metamorphic and the sample has likely undergone significant grain-size reduction due to strain.

Samples from the Big Bear Lake area in the CSBC

JR16-328

This is a sample from coarse-grained tonalitic component to the basement gneisses. It is a foliated tonalite containing a small amount of amphibole, a high proportion of biotite and a majority of quartz and feldspar.

JR16-329

This sample is a granitic gneiss with a medium grain size. It contains very little alteration although many of the feldspars are sericitised. The major minerals are biotite, plagioclase, alkali -feldspar, and quartz, while titanite and apatite are common accessory minerals.

JR16-333

This sample is a medium-grained tonalite that contains a high proportion of amphibole and biotite. Other rock-forming

minerals are plagioclase and quartz, while titanite, apatite, unidentified oxides, and epidote make up accessory minerals. The epidote does not appear to be formed during alteration but occurs as discreet grains within the rock.

Sample from the Brown Lake area in the CSBC

JR16-406

This sample is a medium grained granite that contains biotite, plagioclase, quartz, and alkali feldspar. The biotite is occasionally altered to chlorite, while the feldspars have a moderate degree of sericitization.

Samples from the Patterson Lake area in the CSBC

JR16-512

This sample is a coarse-grained foliated tonalitic-granodioritic rock. It is foliated but not quite gneissic. Biotite content is variable across the outcrop though other aspects of the unit are consistent.

JR16-517

This sample consists of a foliated granite that contains large, potassium-feldspar phenocrysts. The sample also contains biotite, and quartz.

JR16-519

This sample is a medium-to-fine-grained granodiorite that contains biotite, quartz, minor plagioclase, and alkali feldspar as the major minerals. Titanite, apatite, and minor amounts of secondary chlorite make up the obvious accessory minerals. Some grains appear to be relict amphibole that have been altered to epidote and chlorite.

LA-ICPMS Methods

Twenty-two samples with identifiable zircon present in thin section were sent to ZirChron LLC for zircon separation using traditional methods (*e.g.*, magnetic separation, heavy liquids). Zircons returned from these analyses were mounted in epoxy, polished to mid-section and imaged using secondary-electron and backscatter-electron imaging on the Zeiss Auriga field emission SEM at the Carnegie Institution for Science. After imaging, samples were analysed by laser-ablation split-stream methods at the University of Alberta following the methods outlined in Reimink *et al.* (2016b) and summarised below.

Samples were ablated with a Resonetics Excimer 193 nm laser operating with a fluence of ~3 J/cm^2, a spot size of 33 μm, and a repetition rate of 8 Hz. U-Pb isotopic measurements were conducted on a Thermo Element-2XR mass spectrometer using a single secondary electron multiplier detector operating in peak hopping mode. Hafnium isotope compositions were made concurrently on a Thermo Neptune Plus mass spectrometer in multi-collector mode using multiple Faraday detectors fitted with 10^{11} amplifiers. Both U-Pb and Hf datasets were reduced using the Iolite software package in multiple mass spectrometer mode. Both standard and sample analyses were carefully filtered to only integrate sections of the analysis that had consistent U-Pb, Pb-Pb, and Hf-isotope compositions. Each analysis was given a qualitative score to evaluate the quality of the analysis, ranging from 1, meaning very consistent isotope ratios throughout the entire analysis time, to 4, meaning the data was so variable that no meaningful integrations could be used. Final data reduction and calculation of average compositions used only analyses with a 1–3 quality rating to avoid analyses with highly uncertain averages.

Both U-Pb and Hf isotope ratios were normalised to the Plesovice reference material as a primary standard, while zircon 91500, OG1, and in house standard LH91-15 were all monitored as secondary standards. The Yb-interference correction was monitored using MUN1, MUN3, and MUN4 synthetic zircons, each with distinct Yb/Hf ratios, and the apparent $^{173}Yb/^{176}Yb$ ratio was solved by iteratively changing this ratio in the Iolite reduction template such that MUN1, MUN3, and MUN4 zircon analyses returned the accepted $^{176}Hf/^{177}Hf$ ratio (0.282135; Fisher *et al.*, 2011). MUN3 and MUN4 zircon have much greater Yb/Hf than any unknown samples measured here.

All initial $^{176}Hf/^{177}Hf$ and $\varepsilon^{176}Hf$ values, and associated uncertainties, were fully propagated using the algorithms laid out in Ickert (2013). Our best estimate εHf values were calculated by assigning crystallisation ages to each sample. This age was calculated by taking the weighted mean $^{207}Pb/^{206}Pb$ age of the oldest consistent population of analyses, after removing inherited cores. This age was then used to calculate initial εHf values, and associated uncertainties, for all samples. Weighted mean εHf

values were then calculated from this population of analyses. Note that taking a weighted mean after calculating εHf values will ignore systematic uncertainties, however, the primary uncertainty in most of our weighted mean values comes from scatter within a population such that systematic uncertainties would add little extra uncertainty to these values.

One run, Run #4, had excess scatter on the measured Hf-isotope composition of the primary reference material (Plesovice). We interpret this to be due to oxide production within the plasma of the mass spectrometer, as the $^{173}Yb/^{176}Yb$ ratio needed to reproduce the true Hf-isotopic compositions of MUN zircons was different from those used during other sessions, and those commonly required to correct LASS Hf data on the UAlberta Neptune Plus instrument. However, the mean value for all standards during this session was equivalent to the accepted values. As we are using average values for unknown samples, taken from several analyses of co-magmatic zircons, this excess scatter on the standard samples does not affect our ultimate reported age and εHf values for samples run during this time (JR16-103; JR16-213; JR16-215).

Data Reduction Notes

All zircon analyses were rated on a scale of 1–4 based on a qualitative analysis of the quality of the run. These analyses were rated in a similar manner to Reimink *et al.* (2016b) and consisted of evaluating the consistency of measured U/Pb, $^{207}Pb/^{206}Pb$, Lu/Hf, and $^{176}Hf/^{177}Hf$ throughout an analysis. Below we lay out our criterion for ranking a given analysis with the scale of 1–4.

1. Nearly all of the time-resolved analysis had consistent U-Pb and Hf isotope compositions.
2. >50 % of the time-resolved analysis had consistent ages and Hf isotope compositions
3. <50 % of the time-resolved analysis had consistent ages and Hf isotope compositions, but some of the analysis was still consistent and useful
4. No portion of the time-resolved analysis was consistent. Not deemed to be useful information.

We only accepted analyses had analytical qualities that were <4. All data with raw $^{206}Pb/^{204}Pb$ ratios <500 and discordance <-40 were accepted. $^{207}Pb/^{206}Pb$ ages for each sample were calculated with the *weightedmean()* function in IsoplotR (Vermeesch, 2018), using the analyses with the oldest $^{207}Pb/^{206}Pb$ ages and their respective 2SE (propagated).

These 'best estimate' ages were then used to calculate εHf values for each sample. These εHf values were compared to εHf calculated at the $^{207}Pb/^{206}Pb$ age of the actual measurement, and used to evaluate intrinsic εHf variability.

Below, we describe the U-Pb-Hf isotope systematics for each sample, as well as the method used to calculate an age and εHf value for each sample. Uncertainties are calculated using the IsoplotR *weightedmean()* function and thus have two uncertainties reported. The first is the standard deviation and the second is the 95 % confidence interval (Vermeesch, 2018). Where no confidence interval is reported by the calculation, we have replaced with "NA".

U-Pb-Hf Isotope Summary for Each Sample

Acasta Gneiss Complex Samples

JR12-127

All 25 analyses were of acceptable consistency. The seven oldest analyses have consistent 7/6 ages and give a weighted mean age of 3587 ± 14/36 with an MSWD of 2.6. This age is in close agreement with the age determined by Reimink *et al.* (2016a) of 3582 ± 9 Ma, so we used the age determined here for Hf calculations. The weighted mean of the initial $^{176}Hf/^{177}Hf$ of the second through fifteenth analyses is 0.280338 ± 0.000019/0.000041 with an MSWD of 0.19. The weighted mean initial εHf value of the same population is -5.9 ± 0.7/1.5 with an MSWD of 0.43.

JR13-101

Twenty-three of 24 analyses were of acceptable consistency. The six oldest analyses have consistent 7/6 ages and give a weighted mean age of 3684 ± 10/27 with an MSWD of 0.22. This age is significantly younger than the age determined by Reimink *et al.* (2016a) for this sample, 3739 ± 6 Ma, determined by the weighted mean of 18 oldest analyses. We interpret the age of 3739 to be more accurate and therefore used this age to calculate initial Hf values. The weighted mean of the initial $^{176}Hf/^{177}Hf$ from all analyses is 0.280195 ± 0.000019/0.000040 with an MSWD of 0.27. The weighted mean initial εHf value from the oldest 18 analyses is -8 ± 0.9/1.8 with an MSWD of 0.32.

JR13-206

Twelve of 15 analyses were of acceptable consistency. The two oldest analyses have consistent 7/6 ages and give a weighted mean age of 3859 ± 24/NA with an MSWD of 0.054. This age is again significantly younger than the age determined by Reimink *et al.* (2016a) of 3926 ± 30. We used the latter age for Hf calculations as that age came from a weighted mean of the eight oldest ages, as opposed to the two use here. The weighted mean of the initial $^{176}Hf/^{177}Hf$ of the oldest two analyses is 0.280142 ± 0.000072/NA with an MSWD of 0.27. The weighted mean initial εHf value of the same population is -4.7 ± 2.7/NA with an MSWD of 0.31.

JR13-208

Twenty-three of 25 analyses were of acceptable consistency. The nine oldest analyses have consistent 7/6 ages and give a weighted mean age of 3522 ± 12/27 with an MSWD of 0.19. This age is slightly younger than the age determined by Reimink *et al.* (2016), which is 3573 ± 11 Ma, so we used the latter age for calculations. The weighted mean of the initial $^{176}Hf/^{177}Hf$ is 0.280415 ± 0.000022/0.000025 with an MSWD of 0.12 and one outlier rejected. This translates to an initial εHf value of -2.9 ± 0.5 at 3573 Ma.

JR13-304

Twenty-five of 25 analyses were of acceptable consistency. The nine oldest analyses have consistent 7/6 ages and give a weighted mean age of 2931 ± 13/30 with an MSWD of 0.38. This age agrees well with the previously determined age of 2935 ± 9 Ma. The weighted mean of the initial $^{176}Hf/^{177}Hf$ is 0.280705 ± 0.000022/0.000051 with an MSWD of 0.23 and no outliers rejected. This translates to an initial εHf value of -6.8 ± 0.9/2.1 at 2935 Ma.

JR13-802

Twenty-five of 25 analyses were of acceptable consistency. Two analyses had much older ages than the bulk of the igneous population and are interpreted to be xenocrystic cores. The third-thru-seventh oldest analyses have consistent 7/6 ages and give a weighted mean age of 3357 ± 16/52 with an MSWD of 0.65. This age is in good agreement with the previously determined age of this sample (3365 ± 13 Ma), which we use for the Hf-isotope calculations. The weighted mean of the initial $^{176}Hf/^{177}Hf$ is 0.280505 ± 0.000022/0.00007 with an MSWD of 1.4 and zero outliers rejected. This translates to an initial εHf value of -4.0 ± 0.9/2.8 at 3365 Ma with an MSWD of 1.

JR16-101

Eleven out of 19 analyses were of acceptable consistency. The five oldest analyses have consistent 7/6 ages and give a weighted mean age of 3536 ± 14/58.6 with an MSWD of 5.5. The next 6 analyses have 7/6 ages that yield a weighted mean 7/6 age of 3379.1 ± 5.4/15 with an MSWD of 1. The weighted mean initial εHf value of the oldest four analyses (calculated at the measured 7/6 age) of -2.3 ± 0.8/3.3 with an MSWD of 0.7. The weighted mean initial εHf of the next group of analyses is -2.6 ± 0.66/2.1 with an MSWD of 0.41. One outlier was rejected, as it is likely a metamorphic grain, having the same $^{176}Hf/^{177}Hf$ as the older magmatic suite of samples. These Hf-isotope values were calculated using the 7/6 age of the individual analysis.

JR16-102

Twenty-one out of 22 analyses were of acceptable consistency. The sample with the oldest 7/6 age is not obviously an inherited core. The second oldest analysis is not clearly different from other samples with younger 7/6 ages. A weighted mean of analyses 3–9 (in order of 7/6 age) gives an age of 3423.8 ± 5.6/14 with an MSWD of 1.4. A regression has an upper intercept age of 3407 ± 19/39. A weighted mean of the 4–10 oldest analyses gives and initial εHf value of -2.8 ± 1.3/3.3 with an MSWD of 4.7. We treat this as the best estimate of the initial Hf isotope composition of this sample, by removing the grains we interpret to be inherited, and analyses representing Pb-loss from inherited grains.

JR16-103

Twenty-one out of 26 analyses were of acceptable consistency. The oldest analysis had an anomalously old age, though it isn't clearly from a different growth zone. A weighted mean of analyses 4-10 gives an age of 3422.5 ± 4.6/12 Ma with an MSWD of 0.86. A regression through all the data (using option #4 in the *Concordia()* function gives an upper intercept age of 3442.4 ± 5.8/12. The weighted mean initial εHf value of the 4–10 oldest analyses is -0.2 ± 0.9/2.3 with an MSWD of 2.6.

Central Slave Basement Complex Samples

JR16-213

Twenty-eight out of 40 analyses were of acceptable consistency. No obvious cores were found in these samples. The two oldest analyses are from one single grain and may not represent the true age. Therefore, we took a weighted mean of the next four oldest analyses, with an age of 3260 ± 9.1/39.1 Ma and an MSWD of 4.2. The weighted mean initial εHf value of the 3–10 oldest analyses is 1.3 ± 1/2.5 with an MSWD of 1.5.

JR16-215

All 27 analyses were of acceptable consistency. The regression of all data gives an upper intercept age of 2678.4 ± 4.8/9.8. A weighted mean of the 310 analyses gives an age of 2706.2 ± 3.3/7.7 Ma with an MSWD of 0.45. The weighted mean initial εHf value of the oldest 3–13 analyses (with one analysis with low Hf excluded) is 3.7 ± 0.9/2 with an MSWD of 1.8. The low initial εHf value analyses are interpreted to be due to Pb-loss from inherited cores.

JR16-217

All 19 analyses were of acceptable consistency. U-Pb data shows very little scatter, though uncertainties are large, with one analysis having a younger 7/6 age. A weighted mean the 37 analyses gives an age of 2719.1 ± 5.8/18 with an MSWD of 0.86. The weighted mean initial εHf value of the entire population is -1.1 ± 0.5/1 at 2719 Ma with an MSWD of 0.47.

JR16-236

Six out of ten analyses were of acceptable consistency, the weighted mean 7/6 age of all analyses is 3246.2 ± 5.2/14 with an MSWD of 1.1, consistent with ID-TIMS data from other samples of this unit (Ketchum *et al.* unpublished data). The weighted mean initial εHf value of the entire population is 0.6 ± 0.7/2 at 3246.2 Ma with an MSWD of 0.19.

JR16-254

Twenty-two out of 23 analyses were accepted. They fall on a well-defined discordia line, with an upper intercept age of 3165 ± 2.4/4.9. This is slightly older than the weighted mean 7/6 age of the oldest 14 analyses, which is 3136.7 ± 4.9/11 with an MSWD of 0.85. The weighted mean initial εHf value of the entire population is 1.9 ± 0.4/0.8 at 3165 Ma with an MSWD of 0.6.

JR16-328

Thirty analyses out of 33 were accepted. The upper intercept age is 3241.7 ± 2.6/5.3 Ma, matching well with the weighted mean 7/6 age of the oldest 14 analyses, 3239.7 ±2.8/6.1 with an MSWD of 1.1. The weighted mean initial εHf value of the entire population is 0.8 ± 0.4/0.9 at 3241 Ma with an MSWD of 0.37.

JR16-329

Twenty-seven out of 49 analyses were accepted. The upper intercept age is 3312.1 ± 7.5/15 Ma which agrees with the weighted mean 7/6 age of the oldest seven analyses, 3322.6 ± 6/15 Ma with an MSWD of 1.7. The weighted mean initial εHf value of the entire population is 2.5 ± 0.4/0.8 at 3322.6 Ma with an MSWD of 0.7. This is the within uncertainty of the weighted mean initial εHf of the oldest seven analyses (2.7 ± 0.8/2.1, MSWD = 0.74).

JR16-333

All 33 analyses were accepted. The upper intercept age is 3332.8 ± 5/10 Ma. This is slightly older than the weighted mean 7/6 age of the oldest 29 analyses which is 3314 ± 2.5/5.8 with an MSWD of 0.22. The weighted mean of initial εHf value of the entire population is 2.2 ± 0.3/0.7 at 3332 Ma with an MSWD of 0.24.

JR16-406

Twenty-six out of 36 analyses were accepted. The weighted mean 7/6 age of the 2–5 analyses is 2980.2 ± 7.8/25. This age excludes the oldest analysis as an outlier and has an MSWD of 2.2. A second population of analyses 10–17 have a weighted mean 7/6 age of 2891.6 ± 3.9/9.6 Ma with an MSWD of 0.88. These two populations are distinct in their Hf isotope compositions as well as

age. The weighted mean initial εHf at 2980 Ma of the oldest 2–14 analyses is 0.2 ± 0.5/1.1 with an MSWD of 0.7. The weighted mean initial εHf of the rest of the population, calculated at 2891 Ma, is 2.9 ± 0.6/1.2 with an MSWD of 1.5.

JR16-512

Seventeen out of 40 analyses were accepted. A regression of all data yields an upper intercept age of 2946.4 ± 3.6/7.6 Ma. One older analysis has an older 7/6 age and is likely an inherited core. The weighted mean 7/6 age of the oldest 29 analyses is 2927.8 ± 6.7/16 Ma with an MSWD of 2.1. The weighted mean initial εHf value of the entire dataset is -0.4 ± 0.4/0.9 at 2946.4 Ma with an MSWD of 0.41.

JR16-517

Thirty-four analyses out of 47 analyses were of sufficient consistency. The weighted mean 7/6 age of the oldest 6 analyses is 3017 ± 12/49.8 Ma (MSWD = 3.2), in good agreement with the upper intercept of the discordia array, which is 2996 ± 7/15 Ma. The weighted mean initial εHf value of the entire dataset is 3.1 ± 0.4/0.7 at 3017 Ma with an MSWD of 0.61.

JR16-519

Out of 41 analyses, 35 were of sufficient consistency for further evaluation. A weighted mean age of the oldest six analyses gives a 7/6 age of 2998 ± 10/28 Ma with an MSWD of 2.6. This fits well with the upper intercept regression of 3048.6 ± 2.3/4.8 Ma. The weighted mean initial εHf value of all the data points is 1.6 ± 0.3/0.6 at 3048.6 Ma with an MSWD of 1.2.

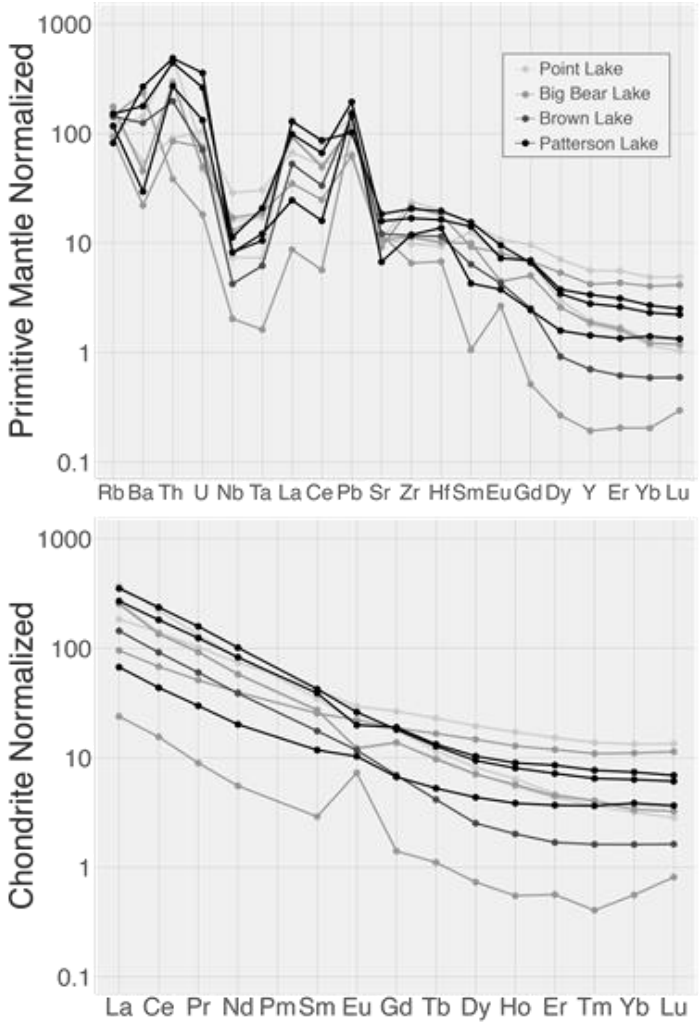

Figure S-2 Trace-element data from CSBC granitoids described here. Samples are divided by location and plotted normalised to primitive mantle (top) and chondrite (bottom) abundances.

Supplemental Methods Regarding U-Pb-Hf Isotope Data Treatment

Several studies have shown that spurious Hf-isotope data can be easily generated (*e.g.*, Amelin *et al.*, 2000; Kemp *et al.*, 2010; Vervoort and Kemp, 2016; and many others). Therefore, care must be taken when making age-εHf assignments to avoid biasing any dataset. Here, we investigated each sample carefully and assigned ages based on the $^{207}Pb/^{206}Pb$ ages, which are minimum age estimates. Below we show two samples as examples of how we approached data reduction.

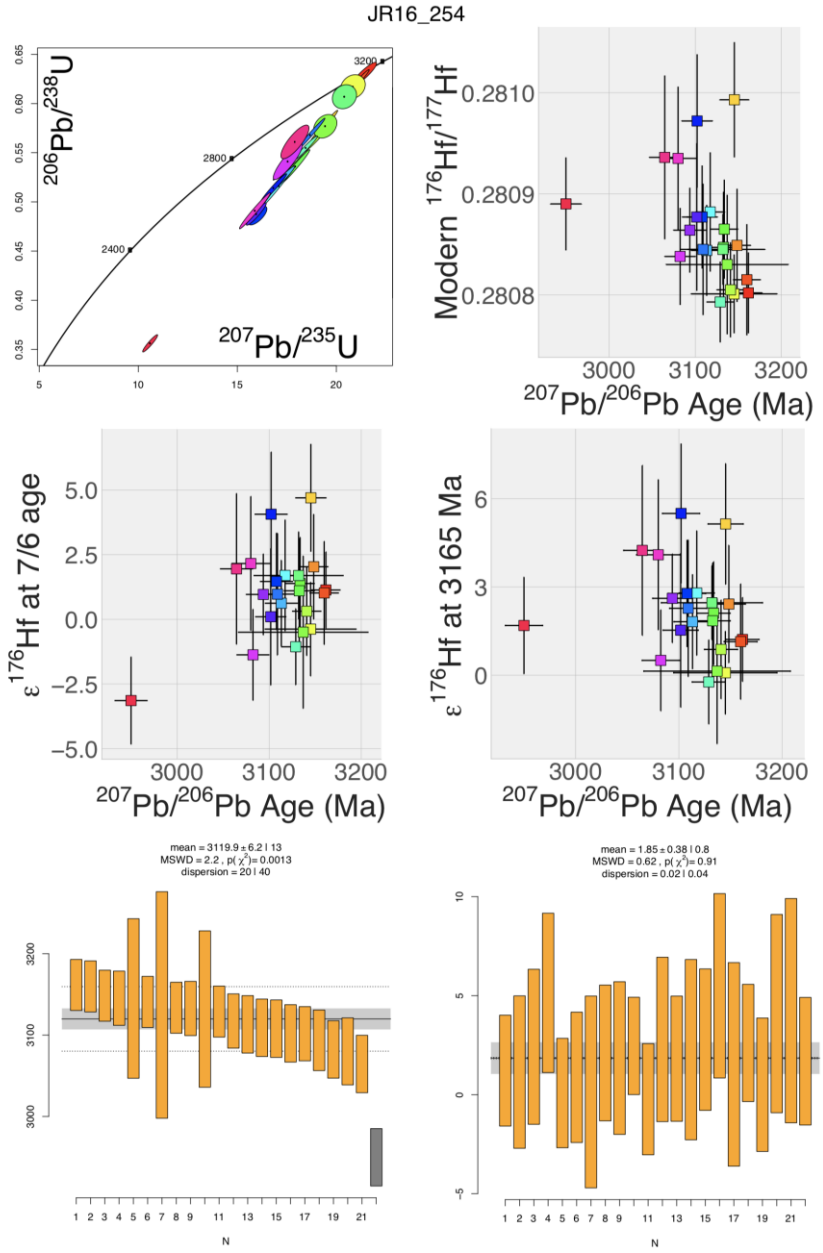

Figure S-3 Split stream U-Pb-Hf data from sample JR16-254. This sample shows relatively simple age-Hf isotope characteristics. The top four panes have individual analyses coloured by analysis number. The U-Pb systematics plot along a relatively simple discordia array. Though several analyses have radiogenic Hf-isotope compositions (high modern $^{176}Hf/^{177}Hf$), these analyses are often higher $^{176}Lu/^{17}Hf$ analyses and get ingrowth corrected down to lower initial values (compare top right with middle left). Correcting all Hf-isotope compositions back to a single age yields a simple εHf population (middle right) whereas when the samples are corrected to the $^{207}Pb/^{206}Pb$ age of the analysis, the εHf value is artificially low (middle left). The bottom two panes are the weighted mean calculations for the $^{207}Pb/^{206}Pb$ ages and εHf values calculated at the best age estimate for the sample (3165 Ma; upper intercept age of the discordia line).

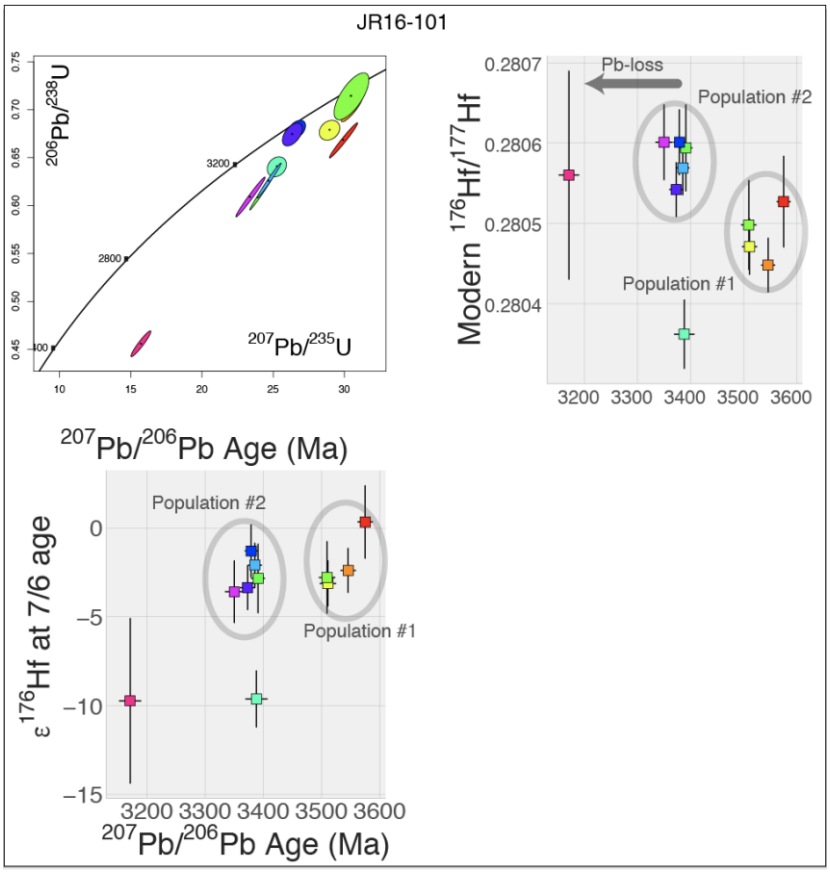

Figure S-4 Split-stream U-Pb-Hf data for sample JR16-101. This sample contains multiple populations of zircon growth, distinguishable by combining the U-Pb and Hf datasets. Symbol colours correspond to individual analyses. The oldest four analyses have distinctly unradiogenic Hf-isotope compositions, suggesting they are a distinct population from the main analyses. Therefore, we broke the analyses into two groups, with distinct ages and εHf values, shown in grey circles. The older population is interpreted to consist of inherited xenocrystic zircon cores, while the second population is interpreted to be the magmatic growth and true age of the rock.

Supplementary Tables

Tables S-1 and S-2 are available for download as Excel files from the online version of the article at http://www.geochemicalperspectivesletters.org/article1907.

Table S-1 Whole-rock major, minor, and trace-element compositions of the samples presented here. The table also includes GPS coordinates for each sample, as well as the average Age and εHf value, determined by zircon LA-ICPMS analysis.

Table S-2 Zircon U-Pb-Hf data. Table S-2a presents the U-Pb-Hf data for standard zircons analysed during each sequence, while Table S-2b presents the U-Pb-Hf isotopic data from the unknowns.

Supplementary Information References

Amelin, Y., Lee, D.C., Halliday, A.N., Pidgeon, R.T. (1999) Nature of the Earth's earliest crust from hafnium isotopes in single detrital zircons. *Nature* 399, 252–255.

Amelin, Y., Lee, D.C., Halliday, A.N. (2000) Early-middle Archaean crustal evolution deduced from Lu-Hf and U-Pb isotopic studies of single zircon grains. *Geochimica et Cosmochimica Acta* 64, 4205–4422.

Bauer, A.M., Fisher, C.M., Vervoort, J.D., Bowring, S.A. (2017) Coupled zircon Lu–Hf and U–Pb isotopic analyses of the oldest terrestrial crust, the >4.03 Ga Acasta Gneiss Complex. *Earth and Planetary Science Letters* 458, 37–48.

Bleeker, W., Ketchum, J.W., Jackson, V.A., Villeneuve, M.E. (1999) The Central Slave Basement Complex, Part I: its structural topology and autochthonous cover. *Canadian Journal of Earth Sciences* 36, 1083–1109, doi: 10.1139/e98-102.

Fisher, C.M., Vervoort, J.D., Hanchar, J.M, (2011) Synthetic zircon doped with hafnium and rare earth elements: A reference material for in situ hafnium isotope analysis. *Chemical Geology* 286, 32–47.

Guitreau, M., Blichert-Toft, J., Martin, H., Mojzsis, S.J. (2012) Hafnium isotope evidence from Archean granitic rocks for deep-mantle origin of continental crust. *Earth and Planetary Science Letters* 337-338, 211–223

Guitreau, M., Blichert-Toft, J., Mojzsis, S.J., Roth, A.S.G., Bourdon, B., Cates, N.L., Bleeker, W. (2014) Lu–Hf isotope systematics of the Hadean–Eoarchean Acasta Gneiss Complex (Northwest Territories, Canada). *Geochimica et Cosmochimica Acta* 135, 251–269.

Ickert, R.B. (2013) Algorithms for estimating uncertainties in initial radiogenic isotope ratios and model ages. *Chemical Geology* 340, 131–138.

Iizuka, T., Hirata, T. (2005) Improvements of precision and accuracy in in situ Hf isotope microanalysis of zircon using the laser ablation-MC-ICPMS technique. *Chemical Geology* 220, 121–137.

Iizuka, T., Komiya, T., Johnson, S.P., Kon, Y., Maruyama, S., Hirata, T. (2009) Reworking of Hadean crust in the Acasta gneisses, northwestern Canada: Evidence from in-situ Lu–Hf isotope analysis of zircon. *Chemical Geology* 259, 230–239.

Kemp, A.I.S., Wilde, S.A., Hawkesworth, C.J., Coath, C.D., Nemchin, A., Pidgeon, R.T., Vervoort, J.D., DuFrane, S.A. (2010) Hadean crustal evolution revisited: New constraints from Pb–Hf isotope systematics of the Jack Hills zircons. *Earth and Planetary Science Letters* 296, 45–56, doi: 10.1016/j.epsl.2010.04.043.

Pietranik, A.B., Hawkesworth, C.J., Storey, C.D., Kemp, A.I.S., Sircombe, K.N., Whitehouse, M.J., Bleeker, W. (2008) Episodic, mafic crust formation from 4.5 to 2.8 Ga: New evidence from detrital zircons, Slave craton, Canada. *Geology* 36, 875–878, doi: 10.1130/G24861A.1.

Reimink, J.R., Chacko, T., Stern, R.A., Heaman, L.M. (2016a) The birth of a cratonic nucleus: lithogeochemical evolution of the 4.02–2.94 Ga Acasta Gneiss Complex. *Precambrian Research* 281, 453–472, doi: 10.1016/j.precamres.2016.06.007.

Reimink, J.R., Davies, J.H.F.L., Chacko, T., Stern, R.A., Heaman, L.M., Sarkar, C., Schaltegger, U., Creaser, R.A., Pearson, D.G. (2016b) No evidence for Hadean continental crust within Earth's oldest evolved rock unit. *Nature Geoscience* 9, 777–780.

Thorpe, R.I., Cumming, G.L., and Mortensen, J.K., 1992, A Significant Pb Isotope Boundary in the Slave Province and Its Probable Relation To Ancient Basement in the western Slave Province. Geological Survey of Canada Open File report, 2484, 179-184.

Vervoort, J.D., Kemp, A.I.S. (2016) Clarifying the zircon Hf isotope record of crust–mantle evolution. *Chemical Geology* 425, 65–75.

Vermeesch, P. (2018) IsoplotR: a free and open toolbox for geochronology. *Geoscience Frontiers*, doi: 10.1016/j.gsf.2018.04.001.

Yamashita, K., Creaser, R.A., Stemler, J.U., Zimaro, T.W. (1999) Geochemical and Nd-Pb isotopic systematics of late Archean granitoids, southwestern Slave Province, Canada: constraints for granitoid origin and crustal isotopic structure. *Canadian Journal of Earth Sciences* 36, 1131–1147, doi: 10.1139/e98-047.